



OPEN ACCESS

EDITED BY Olivier M. Vanakker, Ghent University, Belgium

REVIEWED BY Ronan Padraic Murphy, Dublin City University, Ireland Renzhe Bi,

A*STAR skin research labs (A*SRL), Singapore

*CORRESPONDENCE

Lei Xina

RECEIVED 10 July 2025 ACCEPTED 13 October 2025 PUBLISHED 13 November 2025

Feng L, Liu H, Li Z and Xing L (2025) Colddriven biphasic vascular healing in elderly patients: 4D optical coherence tomography stratification of major adverse cardiovascular event risk based on age-environment interactions.

Front. Cardiovasc. Med. 12:1663394. doi: 10.3389/fcvm.2025.1663394

COPYRIGHT

© 2025 Feng, Liu, Li and Xing. This is an openaccess article distributed under the terms of the Creative Commons Attribution License (CC BY). The use, distribution or reproduction in other forums is permitted, provided the original author(s) and the copyright owner(s) are credited and that the original publication in this journal is cited, in accordance with accepted academic practice. No use. distribution or reproduction is permitted which does not comply with these terms.

Cold-driven biphasic vascular healing in elderly patients: 4D optical coherence tomography stratification of major adverse cardiovascular event risk based on age-environment interactions

Linxing Feng^{1,2}, Huaxing Liu^{1,2}, Zhiyong Li^{1,2} and Lei Xing^{1,2}*

¹Department of Cardiology, The Second Affiliated Hospital of Harbin Medical University, Harbin, China, ²Key Laboratory of Myocardial Ischemia, Ministry of Education, Harbin Medical University, Harbin, China

Background: Biological aging and prolonged cold exposure each impair vascular healing after implantation of a drug-eluting stent. However, their combined effect-particularly in older adults living in cold climates-remains poorly understood.

Objective: To evaluate the joint impact of aging and cold exposure on vascular healing and their association with major adverse cardiovascular events (MACEs) after sirolimus-eluting stent implantation.

Methods: In this retrospective cohort study, 119 patients were stratified into three age groups (≤55, 56-65, and >65 years). Vascular healing was assessed using serial optical coherence tomography (OCT) at 6 and 12 months, with a focus on strut coverage, neointimal hyperplasia (NIH), and spatial heterogeneity. Cold exposure was quantified with the validated Cold Exposure Diary Questionnaire and corroborated by regional meteorological data. The primary end point was the incidence of MACEs at 12 months.

Results: OCT showed delayed endothelialization at 6 months in patients above 65 years compared to younger cohorts (uncovered struts, 11.7% vs. 6.1%; P < 0.001), along with accelerated late-phase NIH progression (3.33 vs. 1.67 μ m/month; P < 0.001). Prolonged cold exposure (>12 h/day) was independently associated with greater neointimal heterogeneity (P = 0.003) and a higher risk of MACEs (hazard ratio, 3.42; 95% CI, 1.65-7.11). A 4D Risk Score, combining OCT-derived healing metrics and cold-exposure data, predicted MACEs; however, external validation is required.

Conclusions: In older patients, the interaction between aging and prolonged cold exposure results in biphasic vascular healing, characterized by early delayed endothelialization followed by excessive neointimal proliferation. The proposed 4-D Risk Score may facilitate individualized risk stratification after percutaneous coronary intervention and warrants prospective validation.

neointimal hyperplasia, drug-eluting stents, optical coherence tomography, aging, cold climate. China

1 Introduction

Drug-eluting stents (DESs) have markedly reduced restenosis and target-lesion revascularization compared with bare-metal stents. Nevertheless, late-phase cardiovascular complications, such as stent thrombosis and recurrent myocardial infarction, remain common, particularly in older adults (1). A principal contributor to these events is delayed vascular healing, typified incomplete endothelialization, uncovered struts, and neointimal heterogeneity (2). This impairment is accentuated in older individuals because of cellular senescence and age-related vascular dysfunction. Optical coherence tomography (OCT), a high-resolution intravascular imaging modality, permits precise evaluation of strut coverage, neointimal thickness, and tissue composition. Serial OCT examinations are therefore invaluable for tracking vascular healing after DES implantation, especially for assessing endothelial recovery and neointimal maturation (3). Nonetheless, the temporal dynamics of vascular healing remain incompletely understood. In particular, biphasic neointimal proliferation—an early plateau followed by delayed regrowth—has not been systematically characterized in high-risk populations. Environmental stressors, such as cold exposure, may further modulate these healing trajectories by interacting synergistically with aging, thereby aggravating endothelial dysfunction and hindering vascular repair. As OCT-derived healing metrics increasingly guide decisions on the duration of dual antiplatelet therapy, there is growing support for a shift from fixed-duration regimens to individualized, image-guided strategies (4).

Mounting evidence highlights considerable inter-individual variability in vascular healing, with older individuals more frequently displaying delayed re-endothelialization and increased neointimal heterogeneity-features closely linked to late-phase complications after stenting (5). While patient and device characteristics well-known contributors, environmental factors—particularly chronic cold exposure—are gaining attention as potential amplifiers of impaired vascular repair. Cold-induced sympathetic activation and vasoconstriction not only impair endothelial function but also increase circulating endothelin-1, a potent vasoconstrictor implicated in vascular dysfunction (6). This cascade may further exacerbate age-related endothelial fragility. Epidemiological data from 27 countries confirm a strong association between ambient cold exposure and cardiovascular mortality (7), and a recent systematic review links chronic low-temperature exposure to increased cardiopulmonary morbidity (8). Despite these associations, the effect of cold exposure on vascular-healing trajectories after DES implantation remains uninvestigated. Moreover, no previous study has integrated objective environmental-exposure metrics longitudinal OCT data in elderly patients undergoing percutaneous coronary intervention (PCI).

The combined effects of aging and cold exposure on vascular health remain poorly understood. Most studies have relied on short-term animal models or retrospective observational data, which do not capture the long-term, synergistic influence of aging and cold exposure on vascular repair. To address this gap, we aimed to determine how aging and cold exposure jointly affect vascular healing in elderly patients after DES implantation and to evaluate their association with major adverse cardiovascular events (MACEs). We hypothesized that cold exposure amplifies age-related delays in vascular healing, thereby increasing the risk of MACEs. By integrating Cold Exposure Diary Questionnaire (CEDQ) data with serial OCT-derived healing metrics, we developed a composite model for predicting MACEs. To our knowledge, this is the first study to combine objective cold-exposure data with OCT assessments of vascular repair in elderly patients, offering novel insights into the implications of aging and cold exposure on vascular healing and the risk of MACEs.

2 Methods

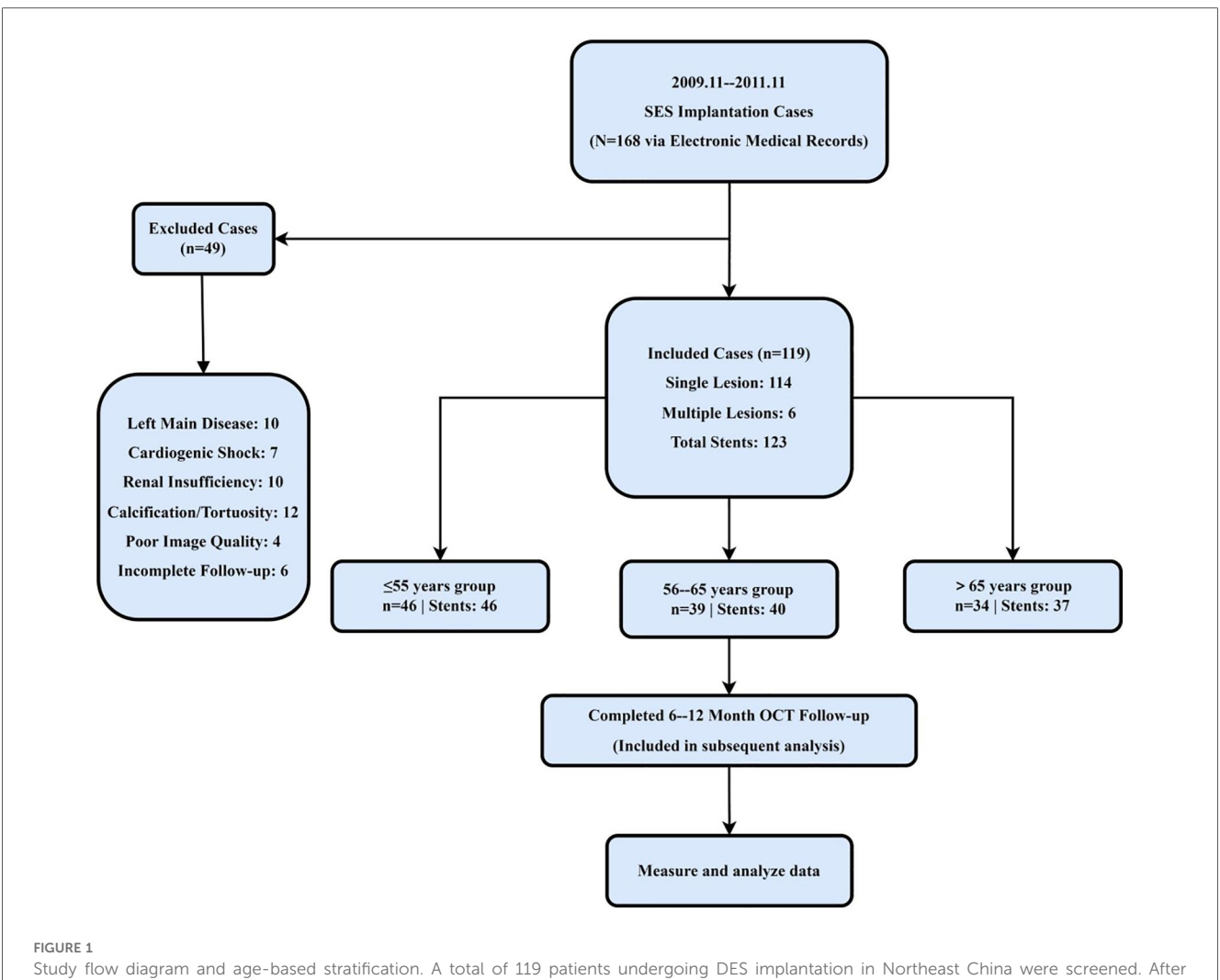
2.1 Patient population

This retrospective cohort study enrolled 119 consecutive patients who underwent elective or urgent PCI with sirolimuseluting stent (SES) implantation between November 2019 and November 2021 in three north-eastern Chinese provinces— Heilongjiang, Jilin, and Liaoning. All patients had a single, de novo coronary lesion; in five cases, overlapping stents were placed within the same target segment. Exclusion criteria were left-main coronary artery disease, symptomatic heart failure (New York Heart Association Class III-IV), renal dysfunction (serum creatinine >1.8 mg/dl), and significant vessel tortuosity or calcification, defined as a calcium arc ≥180° or an intravascular ultrasound calcium score ≥3. Eligible patients were stratified into three age groups on the basis of previously reported age-related differences in neointimal healing and strutcoverage patterns (9): ≤ 55 years (n = 46), 56-65 years (n = 39), and > 65 years (n = 34). The patient screening and exclusion process is summarized in Figure 1. The study was approved by the Ethics Committee of Harbin Medical University, which granted a waiver of informed consent because only anonymized retrospective data were analyzed.

To ensure adequate statistical power for detecting intergroup differences in MACEs, the minimum required sample size was calculated using the following formula for comparing proportions: $n=\frac{Z_{\alpha/2}^2\,P(1-p)}{\delta^2}$, where $Z_{\alpha/2}=1.96$ (two-tailed $\alpha=0.05$), p=0.20 (anticipated MACE incidence), and $\delta=0.10$ (margin of error). The calculated minimum sample size was 62. After accounting for potential data loss and subgroup analyses, a conservative threshold of 102 participants was set and ultimately exceeded by the final cohort of 119 patients.

2.2 Quantitative coronary vessel analysis

Coronary vessel analysis was performed by two independent analysts using QAngio XA (version 7.3). Target segments encompassed the stented regions and the 5-mm proximal and distal margins. Key parameters, including reference vessel



excluding those with left main coronary artery disease, severe calcification, renal dysfunction, or incomplete follow-up, 119 patients were included and stratified into three age groups (≤55, 56−65, >65 years) for longitudinal OCT assessment.

diameter, minimum lumen diameter, percent diameter stenosis, and late lumen loss, were measured according to the standard protocol (10). Inter-reader discrepancies greater than 5% were resolved by consensus.

2.3 OCT image acquisition and analysis

OCT imaging was performed using the LightLab system (version 5.2) with a Dragonfly catheter. The system operated at a center wavelength of 1,310 nm, with an axial resolution of 15 μ m and a lateral resolution of 50 μ m. Pullback images were acquired at 1-mm intervals along each stented segment, excluding side branches \geq 2 mm in diameter, at a pullback speed of 20 mm/s and a frame rate of 100 fps. Saline was used as the flush medium at an injection rate of 4 ml/s. Balloon occlusion was not applied during image acquisition. Image analysis was conducted independently by two reviewers following the ESC 2024 Consensus Guidelines (10). The following definitions and quantitative parameters were applied:

2.3.1 Strut coverage

A strut was classified as uncovered when neointimal coverage was <40 μ m at any follow-up time point, consistent with prior histopathological validation (11). Complete endothelial coverage was defined as a neointimal thickness \geq 40 μ m observed across three consecutive 1-mm cross-sections. Discrepancies between analysts were adjudicated by a third reviewer, resulting in excellent inter-observer agreement (Cohen's κ = 0.85, P < 0.001) (12).

2.3.2 Neointimal heterogeneity

To evaluate age-related differences in neointimal healing, the interquartile range (IQR) of NIH thickness was calculated for each age group (≤55, 56–65, and >65 years). In the elderly group (>65 years), high-risk heterogeneity was defined as an IQR exceeding the 95th percentile of the cohort-wide NIH thickness distribution (13). Because anatomical and healing responses vary by lesion location, the distribution of treated vessels was documented as follows: left anterior descending

(47.2%), left circumflex artery (25.2%), and right coronary artery (27.6%). Lesion location was therefore entered as a covariate in multivariable models to limit confounding. Sensitivity analyses confined to LAD lesions were also performed to test the robustness of spatial-heterogeneity findings. All OCT measurements were obtained using the LightLab system (version 5.2), which showed a strong correlation with histological benchmarks (r = 0.91). Pullback images were acquired at 1-mm intervals along each stented segment, excluding side branches ≥ 2 mm in diameter. Each stent was evaluated in an average of 15 ± 3 cross-sections.

2.3.3 Sampling and analysis

Each frame from the pullback was analyzed, with no frames excluded from analysis. Lumen and stent contours were segmented using a semi-automated approach, with manual adjustments when necessary. Calibration was performed using a standard phantom with known dimensions, and segmentation accuracy was assessed based on inter-scan reproducibility.

2.4 Patient clinical data and follow-up

Follow-up was carried out at 6 and 12 months through outpatient visits and review of electronic medical records. The primary endpoint was the incidence of MACEs, defined as a composite of cardiac death, target-vessel myocardial infarction, or ischemia-driven revascularization. Secondary endpoints included all-cause hospital readmissions and bleeding events classified as Bleeding Academic Research Consortium type ≥2 (14). All clinical events were independently adjudicated by two cardiologists who were blinded to the OCT findings. Complete follow-up data were available for all patients, with no losses reported. The antiplatelet agent prescribed (clopidogrel or ticagrelor) was recorded at baseline and included as a covariate in all multivariable regression models assessing predictors of strut coverage and MACEs.

2.5 Environmental cold exposure assessment

Cold exposure was assessed with the CEDQ, a self-developed instrument that captures outdoor exposure, indoor heating adequacy, and protective behaviors during periods of cold weather. Each item was rated on a 4-point Likert scale (0–3), producing a cumulative score from 0 to 36.

For analytical purposes, a composite cold exposure metric that integrates three components was developed: (1) daily outdoor exposure duration (with individual questionnaire items capped at 8 h to reflect realistic limits for rural and older populations; entries exceeding this threshold were verified by follow-up telephone calls), (2) periods of inadequate indoor heating ($<16\,^{\circ}$ C), and (3) time spent without adequate protective measures during cold weather. High cold exposure was defined as $\geq 12\,\text{h/day}$ of total cold stress accumulated across all three

domains, rather than outdoor time alone. This metric was designed to capture cumulative environmental cold burden rather than any single exposure component.

The previously described protocol demonstrated robust psychometric performance, with a content validity index of 0.92 and a test–retest intraclass correlation coefficient (ICC) of 0.91 (P < 0.001), as well as strong convergent validity with meteorological data (r = 0.82, P < 0.01).

In a subset of participants (n = 34), wearable temperature sensors (iButton DS1922l) recorded skin-proximal temperatures at 10-min intervals over 7 days. Participants spanning a range of age groups, occupations, and housing conditions showed a high level of agreement between CEDQ entries and sensor readings (r = 0.89, P < 0.001), with a bias of 0.7 h/day (limits of agreement: -2.1 to +3.5), supporting the criterion validity of the CEDQ.

Multivariable models assessing the impact of cold exposure on vascular healing were adjusted for two additional covariates: self-reported indoor temperature and a deprivation index derived from postcode-based estimates of housing insulation and household income. A threshold of \leq -20 °C was applied, consistent with the 2022 China Climate Bulletin (15).

2.6 Statistical analysis

Data normality was assessed with the Shapiro–Wilk test. Continuous variables are reported as mean ± standard deviation or median (IQR), as appropriate. For comparisons among three groups, normally distributed variables were analyzed using one-way ANOVA with Bonferroni correction, whereas non-normally distributed data were analyzed with the Kruskal–Wallis test followed by Dunn's *post hoc* analysis. Categorical variables are expressed as counts (%) and compared using the Chi-square test or Fisher's exact test. For two-group comparisons, the Student's *t*-test or the Mann–Whitney *U*-test was applied, depending on data distribution.

Multivariable logistic regression was performed to identify independent predictors of delayed vascular healing and 1-year MACE, with adjustment for age, sex, comorbidities, and stent characteristics. Variables with P < 0.1 in the univariate analysis were entered into the final multivariable model.

Longitudinal changes in NIH were assessed with linear mixed-effects models that included fixed effects for age group, time point, and their interaction, along with random subject intercepts. Inter-observer agreement for NIH measurements and strut coverage was excellent (ICC = 0.92; Cohen's κ = 0.85, P < 0.001).

Time-to-event outcomes were analyzed with Cox proportional-hazards models, adjusted for stent length, duration of diabetes, and serum 25-hydroxyvitamin D [25(OH)D] levels.

To enhance individualized risk stratification after SES implantation—particularly in older patients exposed to environmental cold—we developed a composite prediction tool, the 4D Risk Score.

The model integrates four validated predictors of MACEs: (1) uncovered-strut rate \geq 10%, (2) neointimal growth rate \geq 2.0 μ m/

month; (3) neointimal heterogeneity (IQR) \geq 100 µm, and (4) prolonged cold exposure \geq 72 h at \leq -20 °C (assessed with the CEDQ). Each parameter contributes one point to the total score (range, 0–4). The model was internally validated by receiver-operating-characteristic (ROC) analysis and decision-curve analysis. Risk categories were defined as low (score 0–1), moderate (2–3), and high (4) to guide post-PCI clinical management.

All statistical analyses were performed with SPSS (version 28.0) and R (version 4.2.1); statistical significance was set at P < 0.05.

2.7 Ethical statement

This study was approved by the Ethics Committee of Harbin Medical University. For the cohort of patients who underwent OCT examinations, anonymized retrospective data were used, and therefore, a waiver of informed consent was granted. In contrast, for patients who participated in the cold exposure survey, informed consent was obtained prior to participation. All data were handled in accordance with ethical guidelines, and patient confidentiality was strictly maintained throughout the study.

3 Results

3.1 Baseline characteristics and ageenvironment interactions

In this cohort, 71% of patients received second-generation DES. The baseline demographic, clinical, and environmental characteristics stratified by age group are summarized in Table 1. Elderly patients (> 65 years) experienced significantly longer daily cold exposure (11.5 \pm 4.1 h/day; P < 0.001) and reported lower indoor heating temperatures (20.3 \pm 1.8 °C; P < 0.001) than their younger counterparts. They also had higher fasting glucose concentrations (6.3 \pm 1.4 mmol/L; P = 0.002),

increased low-density lipoprotein cholesterol levels $(2.9\pm0.8~\mathrm{mmol/L};~P=0.019)$, and lower serum $25(\mathrm{OH})\mathrm{D}$ concentrations $(24.6\pm6.2~\mathrm{ng/ml};~P<0.001)$. Collectively, these findings indicate that elderly patients face both metabolic dysregulation and environmental cold stress, which may synergistically impair vascular healing after DES implantation.

3.2 OCT findings: temporal and spatial healing patterns

To evaluate age-related effects on vascular healing, serial OCT assessments were performed at 6 and 12 months. At the 6-month follow-up, younger patients (\leq 55 years) exhibited greater neointimal formation (median NIH thickness: 90 µm, IQR 60–130) and higher strut coverage (72.1%) than elderly patients (median NIH thickness: 60 µm, IQR 50–90; strut coverage: 55.0%; both P<0.001). The elderly cohort also showed the highest proportion of uncovered struts (11.7%), suggesting impaired early endothelialization.

By 12 months, elderly patients displayed a distinct change in healing trajectory, characterized by accelerated neointimal growth (3.33 μ m/month vs. 0.83 μ m/month; P < 0.001) and greater variability in NIH thickness compared with younger patients, indicating a biphasic and disorganized repair pattern.

Age-stratified healing patterns are summarized in Table 2. Patients older than 65 years exhibited significantly delayed endothelialization at 6 months and accelerated NIH progression compared to younger groups (both P < 0.001). Median NIH thickness increased over time in all groups, with the elderly displaying a late-phase catch-up (Figure 2A). The elderly cohort also showed a significantly higher monthly growth rate (Figure 2B). In addition, Figure 2C demonstrates wider IQRs in the elderly, indicating greater neointimal heterogeneity during the late healing phase. Collectively, these findings suggest that advanced age is associated with biphasic, spatially heterogeneous vascular repair after stent implantation. Figure 3 illustrates the hallmark biphasic healing pattern in an elderly patient exposed

TABLE 1 Age-Stratified baseline characteristics and cold exposure metrics.

Variable	≤55 years (n = 46)	56–65 years (n = 39)	>65 years (n = 34)	Overall <i>P</i> -value	Pairwise comparisons
Male, n (%)	30 (65.2%)	22 (56.4%)	19 (55.9%)	0.008*	P1 vs. P2: <i>P</i> = 0.011, P1 vs. P3: <i>P</i> = 0.003
Hypertension, n (%)	21 (45.7%)	33 (84.6%)	29 (85.3%)	<0.001**	P1 vs. P2: <i>P</i> < 0.001, P1 vs. P3: <i>P</i> < 0.001
Fasting glucose (mmol/L)	5.2 ± 0.9	5.8 ± 1.1	6.3 ± 1.4	0.002*	P1 vs. P3: P < 0.001
LDL-C (mmol/L)	2.4 ± 0.7	2.6 ± 0.6	2.9 ± 0.8	0.019*	P1 vs. P3: P = 0.005
Cold exposure (hours/day, ≤-20 °C)	7.8 ± 2.8	9.2 ± 3.3	11.5 ± 4.1	<0.001**	P1 vs. P3: <i>P</i> < 0.001, P2 vs. P3: <i>P</i> = 0.003
Indoor heating temperature (°C)	22.5 ± 1.2	21.8 ± 1.5	20.3 ± 1.8	<0.001**	P2 vs. P3: P = 0.015
Serum 25(OH)D (ng/mL)	32.5 ± 8.7	28.1 ± 7.9	24.6 ± 6.2	<0.001**	P1 vs. P2: <i>P</i> = 0.007, P1 vs. P3: <i>P</i> < 0.001

P1: \leq 55 years; P2: 56–65 years; P3: >65 years.

LDL-C, low-density lipoprotein cholesterol; 25(OH)D, 25-hydroxyvitamin D.

^{*}P<0.05 (significant difference); **P<0.001 (highly significant difference), both based on Bonferroni-corrected threshold. This indicates the observed inter-group differences are unlikely to be caused by random chance, with higher reliability for **.

TABLE 2 Temporal changes in neointimal hyperplasia and strut coverage by Age group.

Parameter/Timepoint	\leq 55 years group ($n = 46$)	56–65 years group (<i>n</i> = 39)	>65 years group (<i>n</i> = 34)	Overall <i>P</i> -value	Pairwise comparisons
6-month follow-up					
Total deployed struts, n	7,057	6,643	5,771	-	-
Analyzable struts, n (%)	6,971 (98.8%)	6,567 (98.9%)	5,633 (97.6%)	0.092	-
Uncovered struts, n (%)	430 (6.1%)	485 (7.3%)	675 (11.7%)	<0.001**	P1 vs. P2: <i>P</i> < 0.001; P1 vs. P3: <i>P</i> < 0.001; P2 vs. P3: <i>P</i> = 0.023
Malapposed struts, n (%)	86 (1.2%)	76 (1.1%)	138 (2.4%)	<0.001**	P1 vs. P3: <i>P</i> = 0.002; P2 vs. P3: <i>P</i> = 0.001
Embedded struts, n (%)	5,085 (72.1%)	3,785 (57.0%)	3,176 (55.0%)	<0.001**	P1 vs. P2: <i>P</i> < 0.001; P1 vs. P3: <i>P</i> < 0.001
NIH thickness (μm), median (IQR) – 6 months	90 (60–130)	60 (40-80)	60 (50–90)	<0.001**	P1 vs. P2: <i>P</i> < 0.001; P1 vs. P3: <i>P</i> < 0.001; P2 vs. P3: <i>P</i> = 0.023
12-month follow-up					
Total deployed struts, n	7,377	6,412	4,610	-	-
Analyzable struts, n (%)	7,281 (98.7%)	6,285 (98.0%)	4,557 (98.9%)	0.156	-
Uncovered struts, n (%)	288 (3.9%)	212 (3.3%)	226 (4.9%)	<0.001**	P1 vs. P3: P < 0.001; P2 vs. P3: P < 0.001
Embedded struts, n (%)	5,629 (76.3%)	4,112 (64.1%)	3,295 (71.5%)	<0.001**	P1 vs. P2: <i>P</i> < 0.001; P1 vs. P3: <i>P</i> = 0.029
NIH thickness (μm), median (IQR) – 12 months	100 (60–150)	70 (50–110)	80 (60–110)	<0.001**	P1 vs. P2: <i>P</i> < 0.001; P1 vs. P3: <i>P</i> < 0.001; P2 vs. P3: <i>P</i> < 0.001
Monthly NIH growth rate (μm/month)	+0.83	+1.67	+3.33	<0.001**	P1 vs. P3: P < 0.001

IQR, interquartile range; NIH, neointimal hyperplasia.

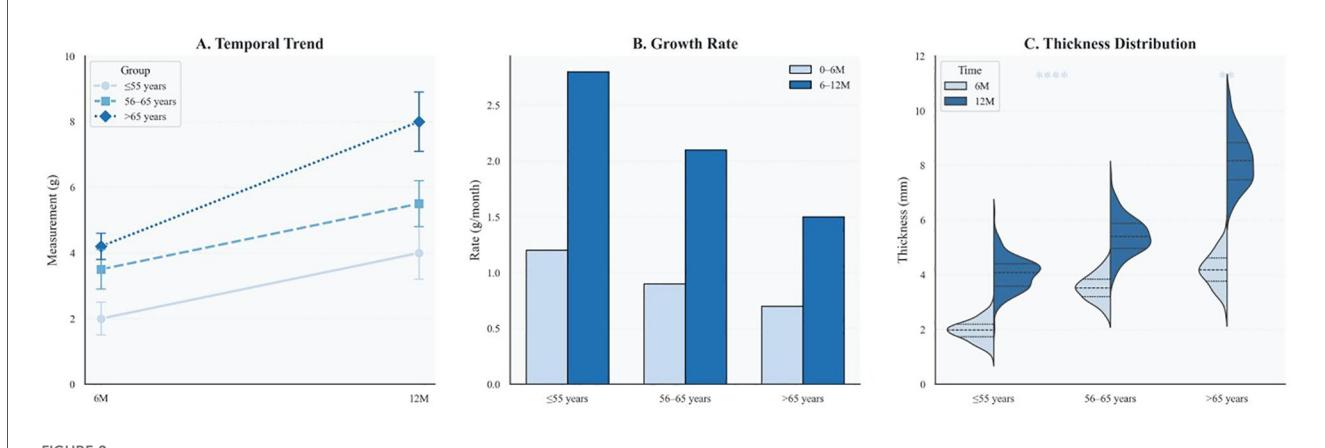
P1: ≤55 years; P2: 56-65 years; P3: >65 years.

Strut analysis excludes struts at major side branches (diameter ≥ 2 mm).

Analyzable struts = total struts minus those with imaging artifacts or at excluded locations.

Monthly growth rate calculated as (12-month thickness - 6-month thickness) ÷ 6 months.

^{*}P < 0.05, **P < 0.01 (Bonferroni-corrected).



Age-specific dynamics of neointimal thickness and distribution over time. (A) Line plot of median neointimal thickness at 6 and 12 months across three age groups, with interquartile ranges shown as error bars. (B) Bar graph comparing neointimal growth rates during early (0-6 months) and late (6-12 months) phases. Color coding corresponds to time intervals and matches those in Panel C. (C) Violin plots display the distribution of neointimal thickness by age group and follow-up time, with quartiles indicated. Statistical significance is annotated (*P < 0.01; **P < 0.0001).

to high levels of cold, showing simultaneous under- and overhealing within a single vessel segment. Figure 4 demonstrates the temporal evolution of three elderly patients with similar cold exposure, revealing pronounced heterogeneity in healing trajectories despite comparable baseline characteristics. The divergent patterns, including delayed coverage (panels A–D), persistent non-healing (panels B–E), and excessive proliferation (panels C–F), were differentially associated with clinical outcomes, with persistent non-healing exhibiting the highest rate of MACEs (45.5% vs. 18.2% for delayed healing, P = 0.023).

These OCT findings provide a foundation for understanding the quantitative impact of cold exposure on clinical outcomes.

3.3 Cold exposure and risk of MACEs: dose-response relationship

Building on the heterogeneous healing patterns observed in elderly patients, we systematically evaluated the dose-response relationship between cold exposure and clinical outcomes. Among

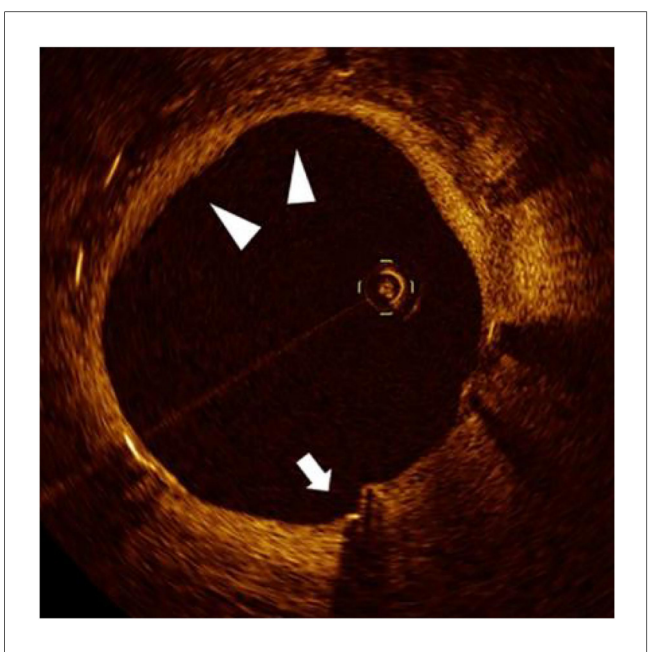


FIGURE 3 Biphasic vascular healing pattern in cold-exposed elderly patient. Representative OCT image from a 71-year-old patient with high cold exposure (CEDQ score 28, >12 h/day at \leq -20 °C) at 12 months post-stent implantation, demonstrating a characteristic biphasic healing response. White arrows indicate persistent uncovered struts, while triangles mark areas of excessive neointimal proliferation within the same cross-section. This paradoxical coexistence of under-healing and over-healing exemplifies the dysregulated vascular repair induced by the synergistic effects of aging and cold exposure.

the 119 participants, cumulative cold exposure during a 7-day period ranged from 28.0 to 64.5 h, with a median of 49.5 h. Individuals exposed to \geq 56 h of ambient cold had a significantly higher incidence of MACEs than those with lower exposure (38.1% vs. 15.5%, P=0.02). A positive association was observed between CEDQ score and MACE risk. In unadjusted logistic-regression analysis, each 1-point increase in CEDQ score was associated with a 24% rise in the odds of MACEs [odds ratio (OR): 1.24, 95% confidence interval (CI): 1.11–1.38, P<0.001]. This relationship remained significant after adjustment for age, sex, comorbidities, indoor temperature, and the residential deprivation index (adjusted OR: 1.21, 95% CI: 1.08–1.35, P<0.001).

Restricted cubic-spline modeling at an ambient temperature of 20 °C demonstrated a near-linear dose–response relationship, whereby each additional hour of exposure to ambient temperatures of 20 °C was associated with a 12% increase in MACE risk (P = 0.012) (Figure 5A). A forest plot of the multivariable-adjusted hazard ratios showed that high daily exposure to cold (\geq 12 h/day, corresponding to the \geq 56 h/week threshold) was linked to a markedly increased risk of MACEs (hazard ratio 3.42, 95% CI: 1.68–6.97, P = 0.001) (Figure 5B). These findings further support a dose-dependent relationship between cold exposure and the occurrence of MACEs.

Table 3 summarizes the full statistical results from the two models. Model A treated the CEDQ score as a continuous variable, whereas Model B categorized cold exposure with a

threshold of 56 h week. Participants in the highest exposure group (\geq 56 h week) had significantly greater odds of MACEs than those in the lowest exposure group (<42 h week; adjusted OR: 2.87, 95% CI: 1.32–6.25, P=0.008). Both models showed significant associations between cold exposure and MACE risk, supporting the predictive validity of both continuous and categorical cold-exposure metrics.

3.4 Predictive value of spatial heterogeneity and the 4d risk score

Spatial heterogeneity of NIH, defined as an IQR >120 μ m, emerged as an independent predictor of MACEs (16). ROC analysis demonstrated moderate discriminative performance, with an area under the curve (AUC) of 0.72. Kaplan–Meier survival analysis confirmed that patients with pronounced spatial heterogeneity had significantly lower MACE-free survival (P < 0.001) (Figure 6).

In the composite 4D Risk Score (Table 4), all four parameters (i.e., uncovered strut rate, neointimal growth rate, spatial heterogeneity, and cold exposure) were independently associated with MACEs, yielding hazard ratios of 2.91, 3.12, 3.42, and 3.25, respectively. The model displayed excellent performance, with an internally validated AUC of 0.83.

A stepwise algorithm illustrating how the 4D Risk Score can inform management after DES implantation is provided in Figure 7. In ROC analysis of the test dataset, the AUC was 0.63 (Figure 8A), indicating only moderate discrimination. This value is lower than initially reported, likely reflecting optimism inherent to internal validation. Nevertheless, decision-curve analysis (Figure 8B) demonstrated a consistent net clinical benefit across a wide range of threshold probabilities, outperforming both "treatall" and "treat-none" strategies and underscoring the clinical utility of the score in optimizing therapeutic decisions. The proposed 4D Risk Score helps in personalized risk assessment and management strategies after PCI. The detailed criteria for scoring and management recommendations are outlined in Table 5.

Collectively, these findings establish the 4D Risk Score as a practical and clinically meaningful tool for individualized risk stratification after PCI, particularly in older patients exposed to environmental cold stress.

4 Discussion

4.1 Biphasic vascular healing pattern

This study identifies a biphasic vascular-healing trajectory in elderly patients after SES implantation in cold environments. This pattern, conceptually illustrated in Figure 9, consists of two distinct phases: In the early phase (0–6 months), healing was markedly delayed, as reflected by higher proportions of uncovered struts and thinner neointimal coverage than in younger adults. During the late phase (6–12 months), neointimal growth accelerated and spatial heterogeneity increased, indicating a

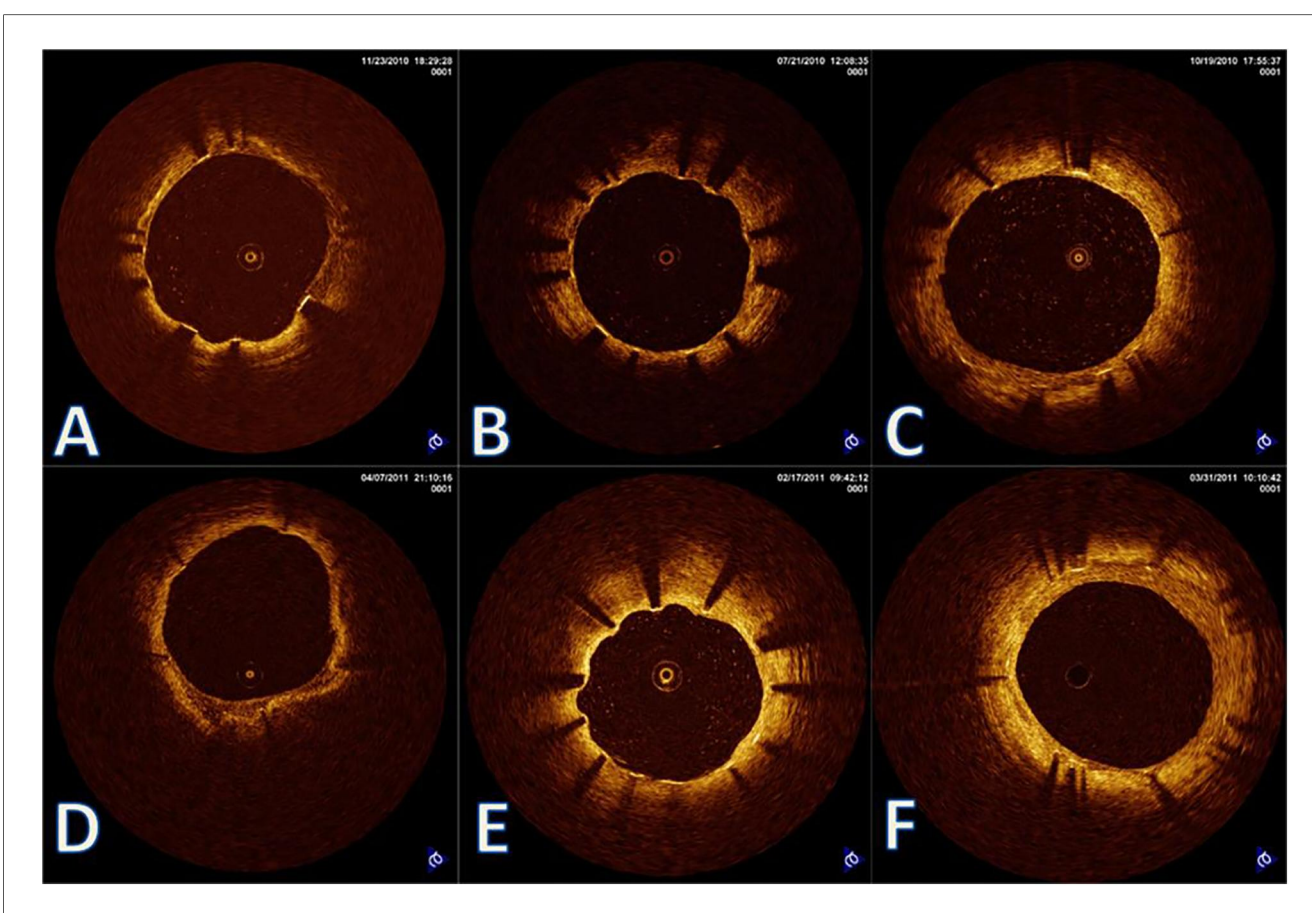


FIGURE 4
Heterogeneous vascular healing trajectories in cold-exposed elderly patients. Representative OCT images from three elderly patients (>65 years) with similar cold exposure levels showing diverse healing outcomes. (A–C) 6-month follow-up; Panels D-F: 12-month follow-up. (A,D) Patient 1: Delayed but eventually adequate healing with thin neointimal coverage at 12 months; (B,E) patient 2: Persistent healing failure with uncovered struts at 12 months (arrows in panel E); (C,F) patient 3: Accelerated healing with complete coverage but excessive neointimal proliferation at 12 months. Despite comparable age and cold exposure, these patients demonstrate the unpredictable nature of vascular healing under environmental stress, highlighting the importance of individualized risk assessment.

compensatory yet dysregulated repair response. Importantly, a dose–response relationship was evident: prolonged cold exposure was associated with a higher uncovered-strut rate and greater neointimal proliferation. These findings suggest that cold exposure functions as a cumulative vascular stressor that amplifies agerelated impairments in endothelial recovery.

The delay in early healing may be driven by cold- and age-induced disruptions of vascular homeostasis. Acute cold exposure precipitates sympathetic over-activation and vasoconstriction by elevating circulating norepinephrine and stimulating α -adrenergic receptors, thereby impairing endothelial reactivity. Chronic cold stress, meanwhile, promotes the release of pro-inflammatory cytokines (e.g., interleukin-6 and tumor necrosis factor- α), leading to delayed endothelial regeneration and destabilized neointimal scaffolding. In addition, mitochondrial dysfunction in endothelial progenitor cells (EPCs) restricts β 1-integrin-mediated migration (17, 18), further contributing to delayed endothelialization.

Aging further exacerbates this dysfunction through telomere attrition, which activates the ataxia-telangiectasia mutated/nuclear serine/threonine protein kinase Chk2/p53 pathway in

vascular smooth muscle cells (VSMCs), leading to G1 cell cycle arrest and a 42% reduction in proliferative capacity compared to younger individuals (19). As a result, neointimal coverage becomes thinner and displays greater spatial heterogeneity (median thickness: $60 \ \mu m$ vs. $90 \ \mu m$; a 75% increase in IQR).

During the chronic phase (6-12 months) of healing, telomeredysfunction-driven stress responses sustain inflammation and epigenetic drift. Up-regulation of the long non-coding RNA TERRA triggers Toll-like receptor-9/nuclear factor κB signaling, enhancing monocyte recruitment and extracellular-matrix remodeling. Concomitantly, hypermethylation of the Krüppellike factor-4 promoter ($\beta > 0.8$) induces phenotypic switching in VSMCs, evidenced by an 80% reduction in the contractile marker α -smooth-muscle actin and a 320% increase in the osteogenic marker osteopontin (20, 21). This phenotypic plasticity drives NIH and metabolic reprogramming via glycolytic enzymes (e.g., 6-phosphofructo-2-kinase/fructoseincreasing cellular-proliferation 2,6-bisphosphatase-3), heterogeneity (IQR $1.7 \rightarrow 4.3$) (22). However, these pathways remain hypothetical because molecular assays (e.g., methylation profiling, RNA sequencing) were not performed. Multivariable

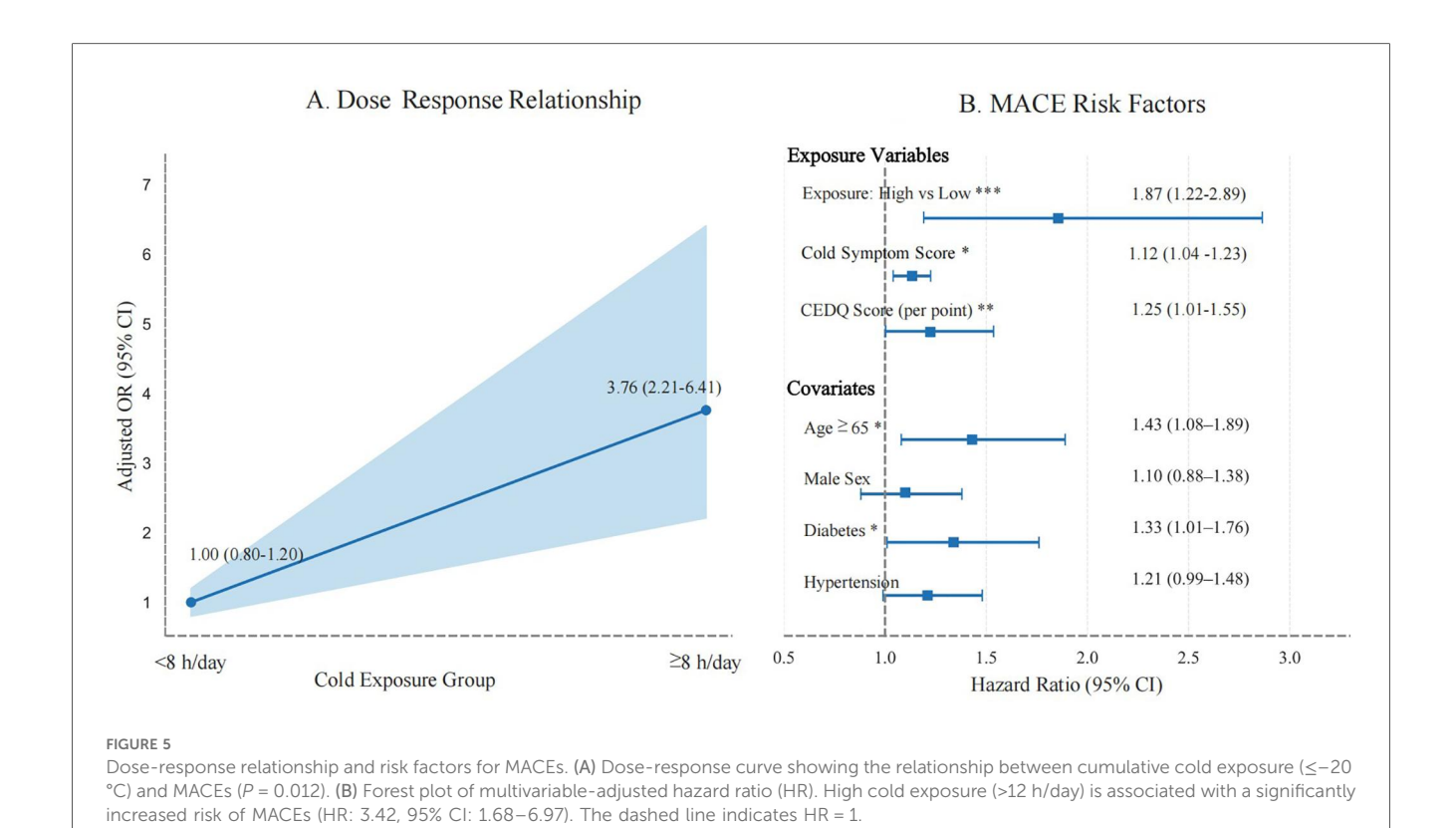


TABLE 3 Dose-Dependent association between cold exposure and MACEs.

Variable	Model A: CEDQ score		Model B: high exposure (≥56 h/week)	
Cold exposure (main variable)	1.21 (1.08–1.35)	P < 0.001	2.87 (1.32-6.25)	P = 0.008
Age ≥65 years	1.42 (0.74-2.73)	P = 0.28	1.38 (0.72-2.64)	P = 0.31
Male sex	1.58 (0.83-3.02)	P = 0.17	1.61 (0.85-3.08)	P = 0.14
Comorbidity index (per point)	1.35 (1.10-1.66)	P = 0.003	1.34 (1.09–1.65)	P = 0.005
Indoor temperature <16 °C	1.93 (1.05-3.53)	P = 0.033	1.85 (1.01-3.41)	P = 0.039
Deprivation index (per SD increase)	1.41 (1.11–1.79)	P = 0.004	1.39 (1.10–1.76)	P = 0.006

MACEs, major adverse cardiovascular events; CEDQ, cold exposure diary questionnaire; SD, standard deviation.

analysis in this study identified aging as an independent predictor of delayed vascular healing, highlighting the need for age-adapted OCT thresholds.

Our results align with those of Tomaniak et al. (23), who reported delayed neointimal coverage in elderly patients at 9 months. Unlike single-time-point studies, we propose a temporal healing trajectory comprising an initial phase of EPC-related dysfunction followed by inflammation-driven HIN. This biphasic pattern, supported by serial OCT data and spatial-heterogeneity metrics, reflects the interplay between aging and cold-induced vascular stress.

4.2 Environmental and aging interactions and risk stratification

Biological aging and chronic cold exposure exert a synergistic "dual-hit" effect on vascular healing, delaying re-

endothelialization and increasing the risk of MACEs. Cold stress promotes oxidative damage and accelerates telomere attrition—two hallmarks of vascular senescence—thereby impairing smooth-muscle repair and endothelial regeneration. In northeastern China, extreme winter conditions intensify vascular vulnerability through two primary mechanisms:

4.2.1 Cold-induced endothelial dysfunction

This dysfunction correlates with CEDQ scores, although mechanistic validation is pending. Wearable thermometric telemetry or flow-mediated dilation testing could provide real-time insights into endothelial function under cold stress.

4.2.2 TRPM8 activation in endothelial and smooth muscle cells (hypothesis)

In endothelial cells, existing literature suggests that TRPM8 activation inhibits vascular endothelial growth factor-mediated angiogenesis by 38% via the Ca²⁺/calcineurin-nuclear factor of

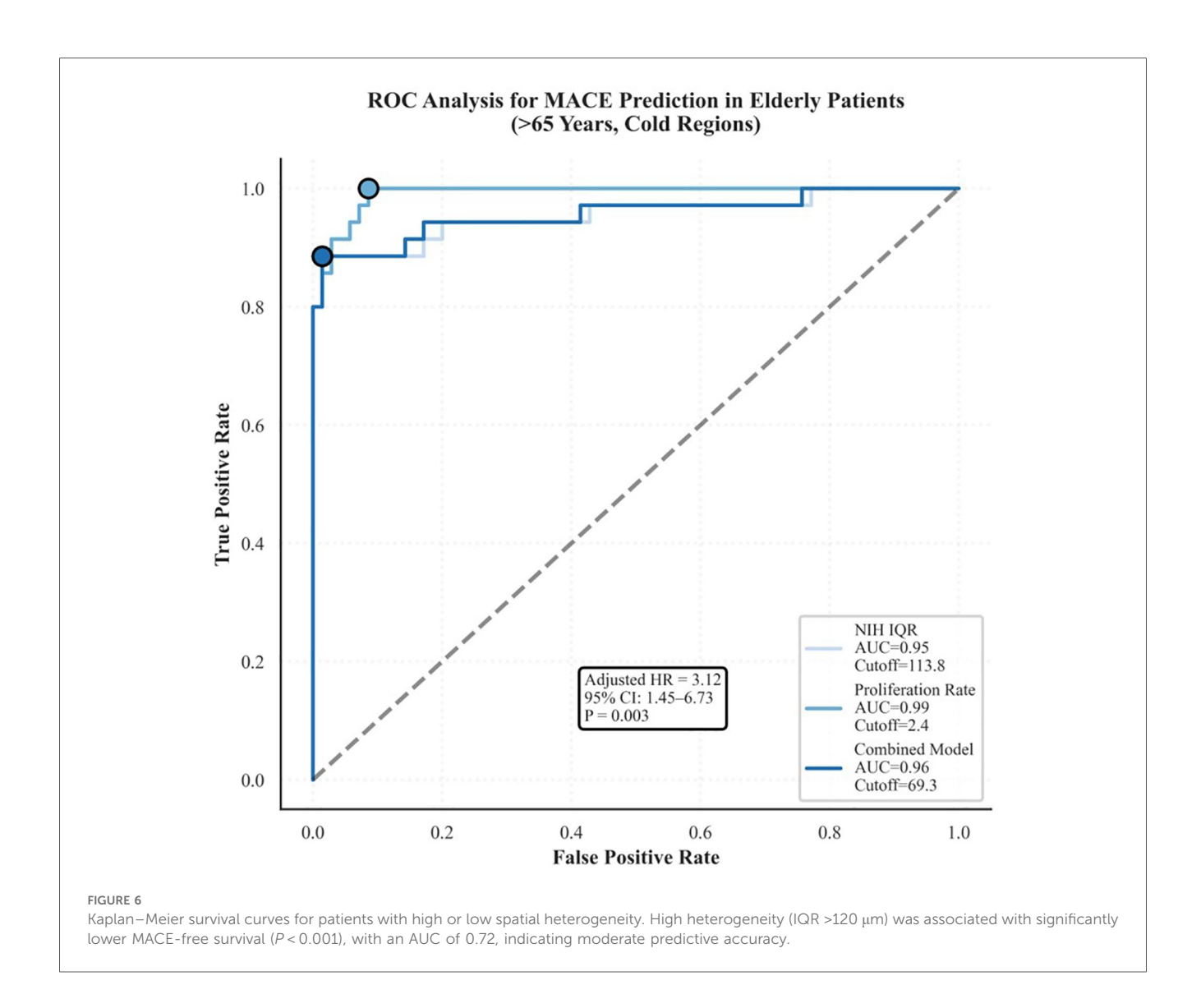


TABLE 4 Multivariable Cox proportional hazards model for cold exposure-related MACE risk.

Exposure type & variable	Adjusted HR	95% CI	P-value
Categorical modeling			
Moderate exposure (8-12 h/day)	1.65	0.98-2.78	0.058
High exposure (>12 h/day)	3.42	1.68-6.97	0.01**
Continuous exposure modeling			
Cold exposure (per 1 h/day increase)	1.12	1.01-1.24	0.012*
Covariates			
Age (per year increase)	1.04	1.01-1.08	0.015*
Male sex	1.12	0.65-1.92	0.670
Hypertension	1.34	0.80-2.22	0.270
Diabetes mellitus	1.45	0.85-2.46	0.175
LDL-C (per 1 mmol/L increase)	1.20	1.02-1.42	0.031*
DAPT duration (per month increase)	0.96	0.91-1.01	0.110

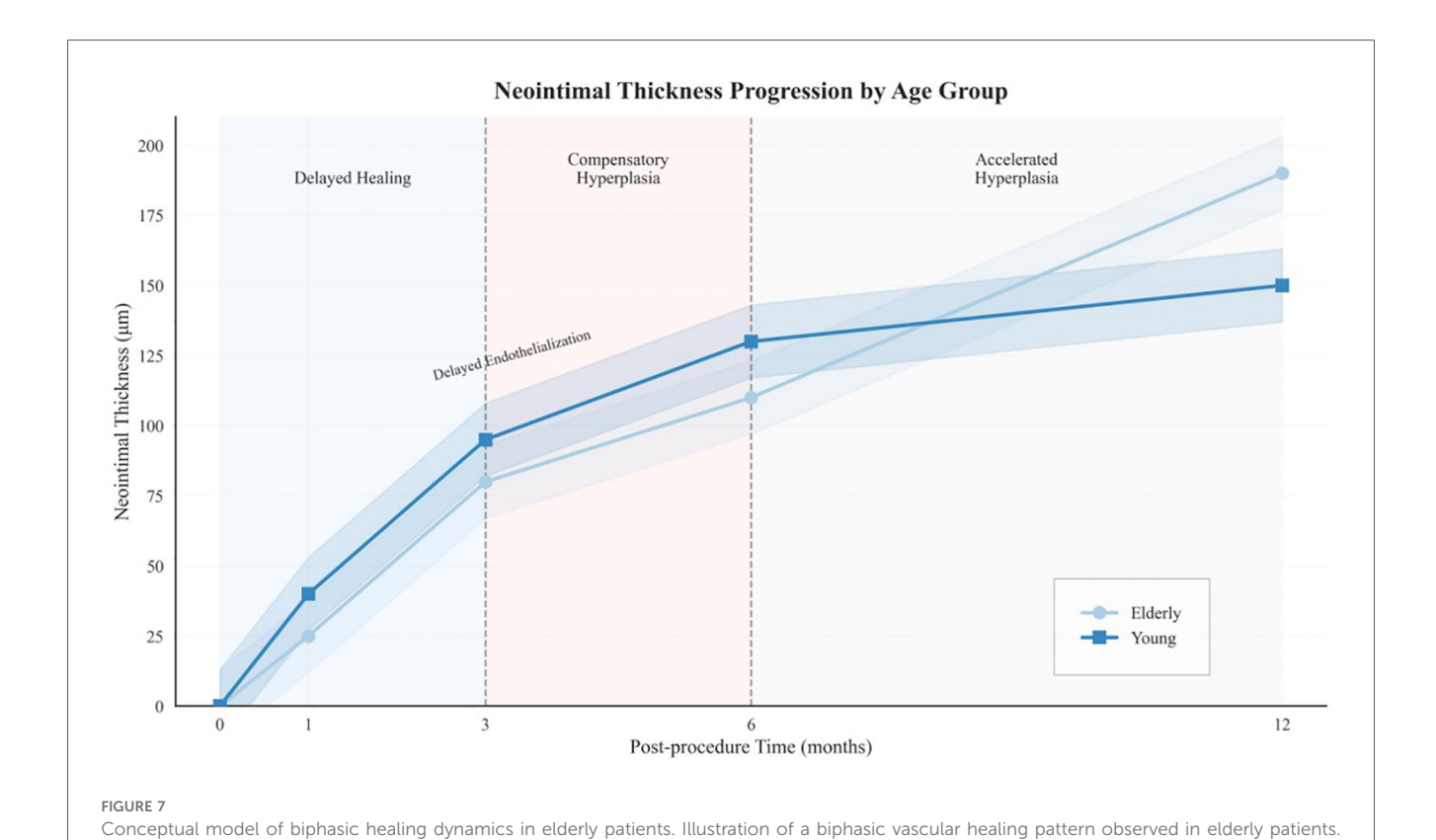
MACE, major adverse cardiovascular event; LDL-C, low-density lipoprotein cholesterol; DAPT, dual antiplatelet therapy.

activated T cells signaling (24, 25). In VSMCs, TRPM8 activation is proposed to enhance ERK1/2 and cyclin-D1 activity, thereby promoting late-phase neointimal growth. These mechanisms are supported by previous studies; however, molecular measurements were not performed in our study and are required for further validation (26).

4.2.3 Air pollution as a compounding stressor

Severe ambient pollution (PM2.5 >150 μ g/m³) further aggravates cold-induced vascular stress through oxidative-injury pathways, producing a 2.3-fold increase in MACE risk relative to temperate regions (P=0.012) (27). In elderly patients, conventional OCT-derived neointimal-thickness thresholds (e.g., \geq 40 μ m) may underestimate healing deficits because focal hyperplasia can mask adjacent uncovered struts, giving false reassurance regarding vascular repair (28, 29). In our cohort, OCT-defined strut coverage correlated only moderately with functional endothelial recovery (r=0.62, P=0.03), highlighting the limitations of OCT alone. Consequently, multimodal

^{*}P < 0.05, **P < 0.01 (Bonferroni-corrected if applicable).



Phase I (0–6 months) is characterized by delayed endothelialization and reduced neointimal formation, whereas Phase II (6–12 months) is marked by exaggerated neointimal proliferation. This pattern reflects the interplay between biological aging and cold-induced vascular stress.

assessments that integrate functional imaging (e.g., fractional flow reserve), inflammatory biomarkers, and quantitative cold-exposure metrics (e.g., CEDQ scores, wearable-sensor data) are warranted (2).

4.3 Limitations

This study has several limitations. First, its retrospective, non-randomized design restricts causal inference, particularly regarding the effect of cold exposure on vascular healing. Second, the choice of antiplatelet therapy (ticagrelor vs. clopidogrel) was not standardized and may have influenced endothelial recovery through distinct platelet-vascular interactions (30). Third, although OCT provides highresolution structural information, it does not capture vascular function (e.g., shear stress, nitric-oxide bioavailability, or endothelial nitric-oxide synthase activity) (31); multimodal imaging (such as fractional flow reserve or near-infrared spectroscopy) should therefore be considered. Fourth, the 12-month follow-up may have missed very-late events, including stent thrombosis or chronic restenosis. Longer-term studies are needed to assess sustained vascular responses to aging and cold exposure. Fifth, although most patients received second-generation DESs (71%), the findings may not be generalizable to third-generation stents or bioresorbable scaffolds, which could differ in healing kinetics under environmental stress (32). Sixth, the elderly subgroup was relatively small (n = 34), limiting the power to detect sexbased differences or gene-environment interactions (e.g., TRPM8 polymorphisms or oestrogen-related endothelial effects) (33). In addition, the absence of physiological measurements (e.g., flow-mediated dilation, circulating endothelial microparticles) limits mechanistic interpretation beyond OCT-derived metrics. Future studies should incorporate such biomarkers to clarify healing heterogeneity. Lastly, while cold-induced vasodilation is known to provide insights into vascular health, this study did not employ noninvasive methods such as diffuse speckle pulsatile flowmetry to assess it. Given its potential as a non-invasive technique to study endothelial function under cold stress, incorporating such methods in future studies could provide valuable additional data and help clarify the mechanisms of vascular healing in response to cold exposure.

5 Conclusion

In elderly patients living in cold climates, a biphasic vascular-healing response after SES implantation was observed: reendothelialization was delayed during the early phase, whereas neointimal proliferation was exaggerated during the late phase. High-resolution OCT revealed substantial spatial heterogeneity, particularly under prolonged cold exposure. These findings indicate a synergistic impact of aging and environmental cold on vascular repair and highlight the need for climate-aware

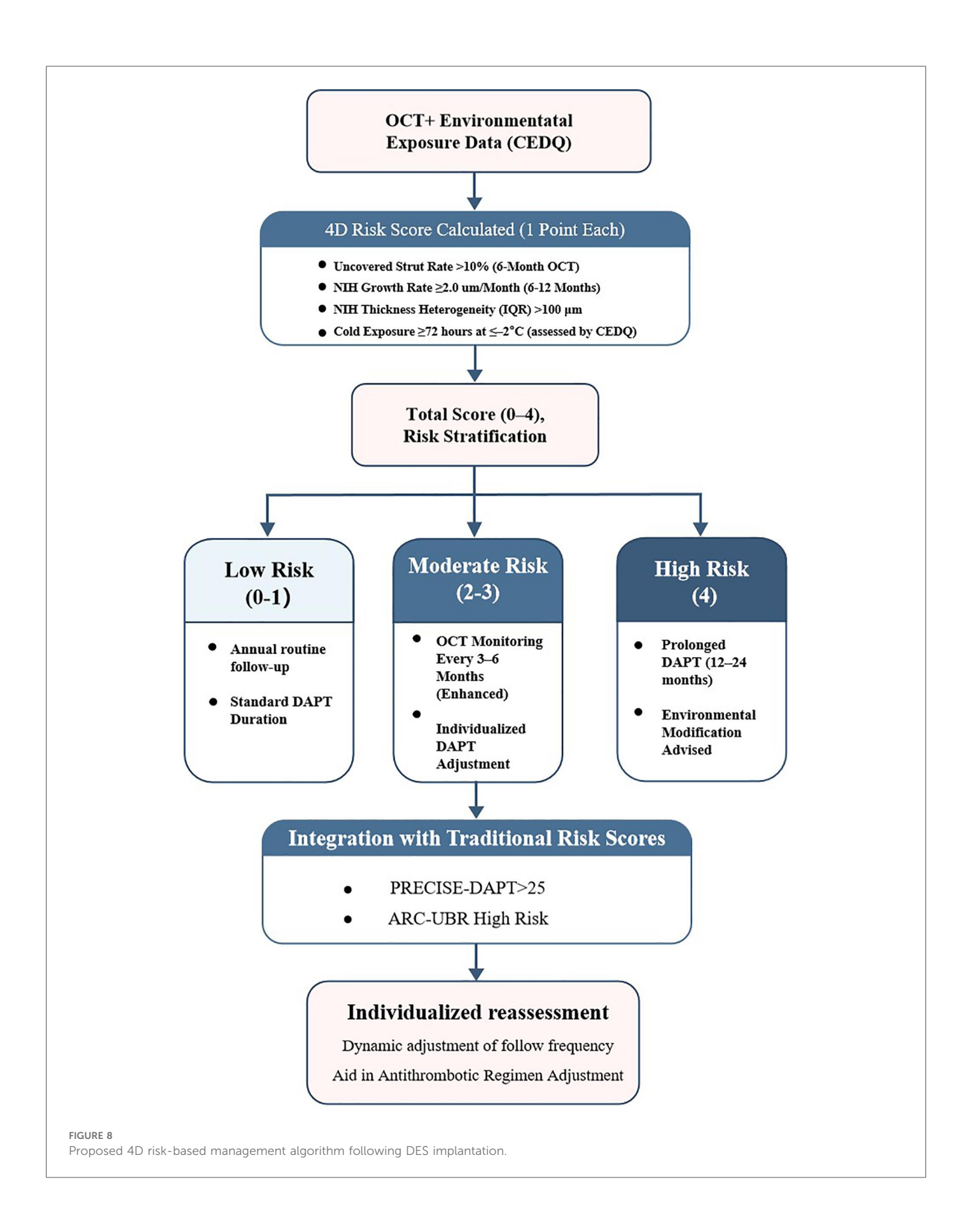
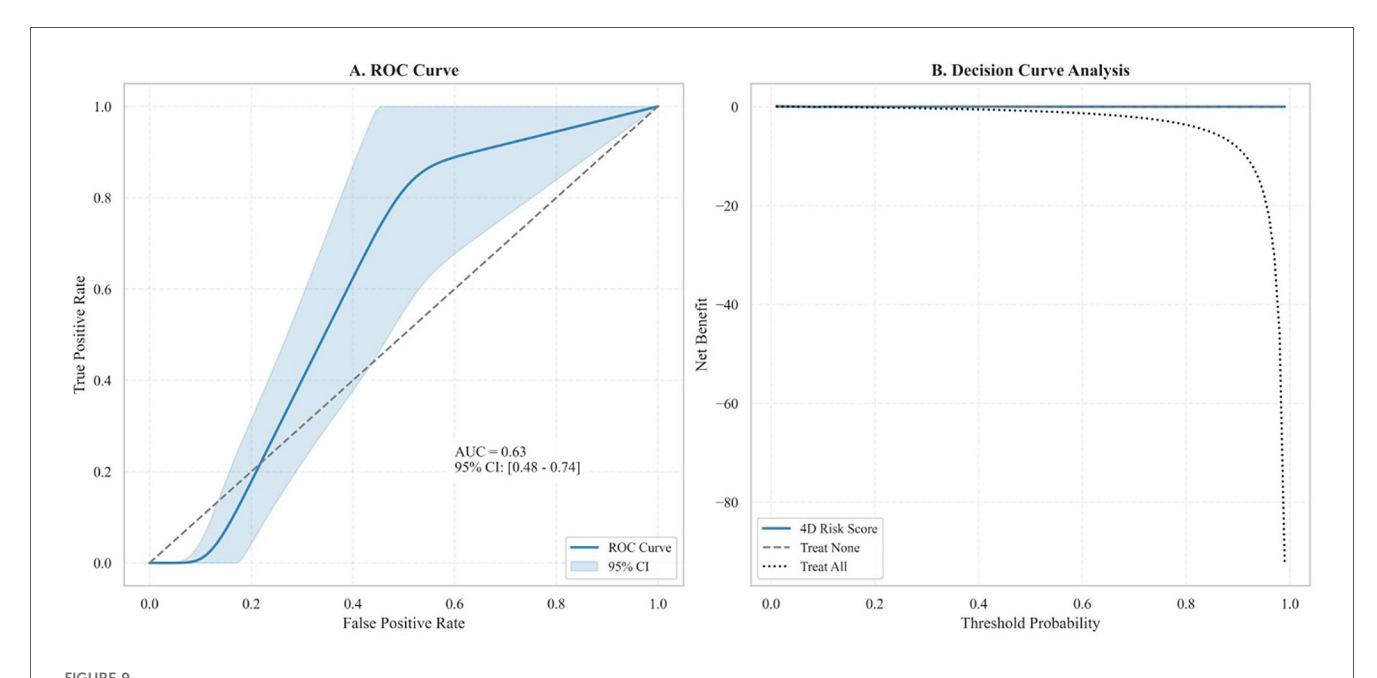


TABLE 5 4D risk score criteria and recommended risk-stratified management.

Parameter	Threshold	Score	Management recommendation	
Uncovered struts	≥10% at 6 months (by OCT)	1	Consider extended DAPT	
Neointimal proliferation rate	>2.0 µm/month at 12 months	1	Intensify OCT follow-up every 3 months	
Neointimal heterogeneity (IQR)	>100 µm	1	Monitor for delayed healing via serial OCT	
Cold exposure (environmental)	≥72 h at ≤-20 °C (assessed by CEDQ)	1	Advise lifestyle changes to reduce exposure	
Total score (0-4)	0-1: Low risk (routine care); 2-3: Moderate risk (enhanced OCT); 4: High risk (intensive follow-up + DAPT adjustment)			

CEDQ, cold exposure diary questionnaire; DAPT, dual antiplatelet therapy; OCT, optical coherence tomography; IQR, interquartile range.



ROC curve analysis and decision curve analysis of the 4D risk score. (A) ROC curve demonstrates the model's discriminatory ability for predicting MACEs (AUC: 0.63, 95% CI: 0.48-0.74; P=0.041). The shaded region delineates the 95% CI. (B) Decision curve analysis shows the net clinical benefit of the 4D Risk Score across varying threshold probabilities. Compared to the "Treat All" and "Treat None" strategies, the model yielded marginal net benefit, primarily at lower thresholds, indicating limited incremental utility in clinical decision-making.

post-PCI surveillance. Preliminary risk modelling that integrates environmental and biological markers showed predictive potential for MACEs, although broader validation is required. Given the study's retrospective design and the small elderly subgroup, the results should be interpreted with caution. Prospective, multicenter studies are warranted to confirm these observations and to inform individualized strategies for vulnerable populations exposed to extreme environmental stress.

Data availability statement

The original contributions presented in the study are included in the article/Supplementary Material, further inquiries can be directed to the corresponding author.

Ethics statement

The studies involving humans were approved by the ethics committee of the Second Affiliated Hospital of Harbin Medical

University (Harbin, China). The studies were conducted in accordance with the local legislation and institutional requirements. The participants provided their written informed consent to participate in this study. Written informed consent was obtained from the individual(s) for the publication of any potentially identifiable images or data included in this article.

Author contributions

LF: Writing – original draft, Writing – review & editing. HL: Data curation, Writing – original draft. ZL: Data curation, Writing – original draft. LX: Project administration, Supervision, Writing – review & editing.

Funding

The author(s) declare that financial support was received for the research and/or publication of this article. This work was supported by the National Key R&D Program of China (Grant

No. 2023YFC2506503, Intelligent Assessment of Coronary Atherosclerosis via Non-Invasive CT Technology) and the Fund of Key Laboratory of Myocardial Ischemia, Ministry of Education (Grant No. KF202214).

Conflict of interest

The authors declare that the research was conducted in the absence of any commercial or financial relationships that could be construed as a potential conflict of interest.

Generative AI statement

The author(s) declare that no Generative AI was used in the creation of this manuscript.

Any alternative text (alt text) provided alongside figures in this article has been generated by Frontiers with the support of artificial intelligence and reasonable efforts have been made to

ensure accuracy, including review by the authors wherever possible. If you identify any issues, please contact us.

Publisher's note

All claims expressed in this article are solely those of the authors and do not necessarily represent those of their affiliated organizations, or those of the publisher, the editors and the reviewers. Any product that may be evaluated in this article, or claim that may be made by its manufacturer, is not guaranteed or endorsed by the publisher.

Supplementary material

The Supplementary Material for this article can be found online at: https://www.frontiersin.org/articles/10.3389/fcvm.2025. 1663394/full#supplementary-material

References

- 1. Lim S, Choo EH, Choi IJ, Kim JS, Kim HK, Jeon HK, et al. Risks of recurrent cardiovascular events and mortality in 1-year survivors of acute myocardial infarction implanted with newer-generation drug-eluting stents. *J Clin Med.* (2021) 10(16):3549. doi: 10.3390/jcm10163549
- 2. Nakata T, Fujii K, Fukunaga M, Nishimura Y, Okada M, Oka T, et al. Morphological, functional, and biological vascular healing response 6 months after drug-eluting stent implantation: a randomized comparison of three drug-eluting stents. *Catheter Cardiovasc Interv.* (2016) 88(3):350–7. doi: 10.1002/ccd.26527
- 3. Ishida M, Terashita D, Itoh T, Shiono Y, Otake H, Kawamoto H, et al. Vascular response occurring at 3 months after everolimus-eluting cobalt-chromium stent implantation in patients with ST-segment elevation myocardial infarction vs. stable coronary artery disease. *Circ J.* (2020) 84(11):1941–8. doi: 10.1253/circj.CJ-20-0386
- 4. Itoh T, Otake H, Kimura T, Shirai S, Yamanaka F, Kadota K, et al. Serial optical frequency-domain imaging study of early and late vascular responses to bioresorbable-polymer sirolimus-eluting stents for the treatment of acute myocardial infarction and stable coronary artery disease patients: results of the MECHANISM-ULTIMASTER study. *Cardiovasc Interv Ther.* (2022) 37(2):281–92. doi: 10.1007/s12928-021-00842-0
- 5. Matsuura T, Ueno M, Watanabe H, Ozawa T, Konishi H, Takahashi K, et al. Impact of neointimal condition and platelet reactivity on intrastent thrombus at long-term follow-up after 2nd- and 3rd-generation drug-eluting stent implantation—insights from a coronary angioscopy and pharmacodynamic study. *Circ J.* (2020) 84(12):2244–52. doi: 10.1253/circj.CJ-20-0554
- 6. Guan WX, Lan Z, Wang QC, Liu Y, Zhang P, Li J, et al. Effects of prolonged cold stress on vascular function in Guinea pigs with atherosclerosis. *J Cardiovasc Pharmacol.* (2025) 85(1):63–74. doi: 10.1097/FJC.0000000000001498
- 7. Alahmad B, Khraishah H, Roye D, Gasparrini A, Karamitri M, Zanobetti A, et al. Associations between extreme temperatures and cardiovascular cause-specific mortality: results from 27 countries. *Circulation*. (2023) 147(1):35–46. doi: 10.1161/CIRCULATIONAHA.122.060903
- 8. Zafeiratou S, Samoli E, Dimakopoulou K, Rodopoulou S, Analitis A, Atkinson RW, et al. A systematic review on the association between total and cardiopulmonary mortality/morbidity or cardiovascular risk factors with long-term exposure to increased or decreased ambient temperature. *Sci Total Environ.* (2021) 772:145383. doi: 10.1016/j.scitotenv.2020.145383
- 9. Takano M, Inami S, Jang IK, Yamamoto M, Murakami D, Okamatsu K, et al. Evaluation by optical coherence tomography of neointimal coverage of sirolimus-eluting stent three months after implantation. *Am J Cardiol.* (2007) 99(8):1033–8. doi: 10.1016/j.amjcard.2006.11.055
- 10. Vrints C, Andreotti F, Koskinas KC, Bax JJ, Benzer W, Bugiardini R, et al. 2024 ESC guidelines for the management of chronic coronary syndromes. *Eur Heart J.* (2024) 45(36):3415–537. doi: 10.1093/eurheartj/ehad575
- 11. Taniwaki M, Radu MD, Zaugg S, Amabile N, Garcia-Garcia HM, Yamaji K, et al. Mechanisms of very late drug-eluting stent thrombosis assessed by optical

- coherence tomography. *Circulation*. (2016) 133(7):650–60. doi: 10.1161/CIRCULATIONAHA.115.019710
- 12. Landis JR, Koch GG. The measurement of observer agreement for categorical data. Biometrics.~(1977)~33(1):159-74.~doi:~10.2307/2529310
- 13. Stone GW, Maehara A, Lansky AJ, de Bruyne B, Cristea E, Mintz GS, et al. A prospective natural-history study of coronary atherosclerosis. N Engl J Med. (2011) 364(3):226-35. doi: 10.1056/NEJMoa1002358
- 14. Mehran R, Rao SV, Bhatt DL, Gibson CM, Caixeta A, Eikelboom J, et al. Standardized bleeding definitions for cardiovascular clinical trials: a consensus report from the bleeding academic research consortium. *Circulation*. (2011) 123(23):2736–47. doi: 10.1161/CIRCULATIONAHA.110.009449
- 15. China Meteorological Administration. *China Climate Bulletin 2022*. Beijing: China Meteorological Press (2023).
- 16. Nerlekar N, Ha FJ, Cheshire C, Gulati A, Yeang C, van Gaal WJ, et al. Computed tomographic coronary angiography-derived plaque characteristics predict Major adverse cardiovascular events: a systematic review and meta-analysis. *Circ Cardiovasc Imaging*. (2018) 11(1):e006973. doi: 10.1161/CIRCIMAGING.117. 006973
- 17. Li DW, Liu ZQ, Wei J, Liu Y, Hu LS. Contribution of endothelial progenitor cells to neovascularization (review). *Int J Mol Med.* (2012) 30(5):1000–6. doi: 10. 3892/ijmm.2012.1073
- 18. Ahmed B, Rahman AA, Lee S, Malhotra R. The implications of aging on vascular health. Int J Mol Sci. (2024) 25(20):10943. doi: 10.3390/ijms252010943
- 19. Ya J, Bayraktutan U. Vascular ageing: mechanisms, risk factors, and treatment strategies. Int J Mol Sci. (2023) 24(14):11508. doi: 10.3390/ijms241411508
- 20. Wu Q, Hu Z, Wang Z, Zhang Y, Ji L, Liu C, et al. Glut10 restrains neointima formation by promoting SMCs mtDNA demethylation and improving mitochondrial function. *Transl Res.* (2023) 260:1–16. doi: 10.1016/j.trsl.2023.02.003
- 21. Koch Z, Li A, Evans DS, Cummings S, Ideker T. Somatic mutation as an explanation for epigenetic aging. *Nat Aging*. (2025) 5(1):45–58. doi: 10.1038/s43587-024-00672-1
- 22. Almacellas E, Pelletier J, Manzano A, García-Rocha M, Ambrosio S, de la Rosa AJ, et al. Phosphofructokinases axis controls glucose-dependent mTORC1 activation driven by E2F1. *iScience*. (2019) 20:434–48. doi: 10.1016/j.isci.2019.09.045
- 23. Tomaniak M, Kołtowski Ł, Pietrasik A, Bagienski M, Maciejczyk M, Kochman J, et al. Serial 3- and 9-year optical coherence tomography assessment of vascular healing response to sirolimus- and paclitaxel-eluting stents. *Int J Cardiovasc Imaging*. (2019) 35(1):9–21. doi: 10.1007/s10554-018-1457-0
- 24. Pandics T, Major D, Fazekas-Pongor V, Varga Z, Tabák ÁG, Kunos L, et al. Exposome and unhealthy aging: environmental drivers from air pollution to occupational exposures. *Geroscience*. (2023) 45(6):3381–408. doi: 10.1007/s11357-023-00854-7

- 25. Das UN. Potential role of TRPM8 in cold-induced hypertension and its clinical implications. *Discov Med.* (2023) 35(177):451-7.
- 26. Huang F, Ni M, Zhang JM, Li DJ, Shen FM. TRPM8 downregulation by angiotensin II in vascular smooth muscle cells is involved in hypertension. *Mol Med Rep.* (2017) 15(4):1900–8. doi: 10.3892/mmr.2017.6321
- 27. Ho CC, Chen YC, Tsai MH, Hsiao TC, Yang YL, Tseng CJ, et al. Ambient particulate matter induces vascular smooth muscle cell phenotypic changes via NOX1/ROS/NF-κB dependent and independent pathways: protective effects of polyphenols. *Antioxidants (Basel)*. (2021) 10(5):742. doi: 10.3390/antiox10050742
- 28. Xhepa E, Byrne RA, Rivero F, Kufner S, Cassese S, Ndrepepa G, et al. Qualitative and quantitative neointimal characterization by optical coherence tomography in patients presenting with in-stent restenosis. *Clin Res Cardiol.* (2019) 108(9):1059–68. doi: 10.1007/s00392-019-01449-7
- 29. Karanasos A, Simsek C, Gnanadesigan M, van Ditzhuijzen NS, Freire R, Diletti R, et al. OCT assessment of the long-term vascular healing response 5 years after

- everolimus-eluting bioresorbable vascular scaffold. J
 Am Coll Cardiol. (2014) 64(22):2343–56. doi: 10.1016/j.jacc.2014.09.032
- 30. Albadrani MS, Elhusein AM, Alotaibi YA, Alqarni AA, Alghamdi SA, Al-Mansouri NM, et al. Efficacy of ticagrelor compared to clopidogrel in improving endothelial function in patients with coronary artery disease: a systematic review. *J Cardiovasc Med (Hagerstown)*. (2022) 23(9):589–96. doi: 10.2459/JCM.00000000000001334
- 31. Boughaleb H, Lobysheva I, Dei ZF, Balligand JL, Montiel V. Biological assessment of the NO-dependent endothelial function. *Molecules*. (2022) 27(22):7997. doi: 10.3390/molecules27227997
- 32. Miura T, Sonoda S, Sanuki Y, Nishizawa J, Horiuchi M, Higashikuni Y, et al. Comparison of post-stent irregular protrusion and subsequent neointimal characteristics between second- and third-generation drug-eluting stent implantation. *J Cardiol.* (2020) 76(5):464–71. doi: 10.1016/j.jjcc.2020.05.013
- 33. SenthilKumar G, Katunaric B, Bordas-Murphy H, Sarvaideo J, Freed JK. Estrogen and the vascular endothelium: the unanswered questions. *Endocrinology*. (2023) 164(6):bqad061. doi: 10.1210/endocr/bqad061